AIAA JOURNAL
Vol. 42, No. 12, December 2004

Calculation of Supersonic Combustion Using Implicit Schemes

Seokkwan Yoon*
NASA Ames Research Center, Moffett Field, California 94035

Scramjet is an essential mode of operation for airbreathing rocket propulsion systems. Both fully and loosely coupled iterative methods, in conjunction with Gauss–Seidel relaxation, have been compared for supersonic combustion calculations. The effect of the Jacobian of source terms on stability and convergence has been investigated. Convergence rates have been compared for loosely and fully coupled implicit schemes. Results include the effects of chemical reaction and Mach numbers on convergence. Robustness of the numerical method has been demonstrated for a test case with staged fuel injection.

Nomenclature

A, B, C	=	Jacobian matrices of convective flux vectors
a_i	=	coefficients for a fourth-order polynomial of temperature of species i
C_i	=	mole concentration of species i
C_{p_i}	=	mass-averaged specific heat at constant pressure of species i
C_{p_m}	=	specific heat at constant pressure of gas mixture
C_{v_i}	=	mass-averaged specific heat at constant volume of species i
D_x, D_x^+, D_x^-	=	central, forward, and backward difference operators
d	=	artificial dissipation
$\boldsymbol{E}, \boldsymbol{F}, \boldsymbol{G}$	=	convective flux vectors
$\boldsymbol{E}_v, \boldsymbol{F}_v, \boldsymbol{G}_v$	=	viscous flux vectors
e	=	internal energy of gas mixture
H	=	Jacobian matrix of source term
h_i	=	enthalpy of species i
h_{fi}	=	heat of formation of species i
I	=	identity matrix
K^f, K^b	=	forward and backward reaction rate coefficients
L, D, U	=	lower, diagonal, and upper factors
N	=	the number of species
N_R	=	the number of elementary reactions
p	=	pressure
$\boldsymbol{Q}$	=	vector of conserved variables
R	=	universal gas constant
$\boldsymbol{S}$	=	source term
T	=	temperature
t	=	time
$\boldsymbol{u}$	=	velocity
W_i	=	molecular weight of species i
X_i	=	mole fraction of species i
Y_i	=	mass fraction of species i
α	=	time step coefficient
β	=	coefficient for artificial dissipation
γ	=	equivalent specific heat ratio
μ	=	viscosity
ν', ν''	=	stoichiometric coefficients
ρ	=	density
τ	=	third body efficiency correction coefficients
ϕ	=	flux limiter
ψ_{ij}	=	intercollision parameter
$\dot{\omega}$	=	rate of change of species concentration

Received 18 June 2003; presented as Paper 2003-3546 at the AIAA 16th Computational Fluid Dynamics Conference, Orlando, FL, 23–26 June 2003; revision received 25 May 2004; accepted for publication 16 July 2004.

*Research Scientist, Advanced Supercomputing Division.

I. Introduction

ONE of the technology goals of NASA for advanced space transportation is to develop highly efficient propulsion systems to reduce the cost of payload for space missions. Development of rockets for the second-generation reusable launch vehicle (RLV) in the past decade has been focused on low-cost versions of conventional engines. Current plans emphasize using human-rated expendable rockets to launch a crew exploration vehicle partly to meet the requirement of retiring the space shuttle fleet by 2010. However, recent interest and success in scramjet engines for military applications such as hypersonic cruise missiles might suggest that airbreathing rockets could reemerge as a possible propulsion system for the next generation RLV. Whereas the weight of the oxygen tank exceeds 30% of the total weight of the space shuttle at launch, only 1% of the total weight is for the payload. Airbreathing rocket propulsion systems, which consume oxygen in the air, offer clear advantages by making vehicles lighter and more efficient.

Experience in the National Aerospace Plane Program in the late 1980s indicates that scramjet engines can achieve high specific impulse for low hypersonic vehicle speeds. Whether using a form of rocket-based combined cycle or turbine-based combined cycle, the scramjet is an essential mode of operation for airbreathing rockets. It is well known that fuel–air mixing and rapid combustion are of crucial importance for the success of scramjet engines because the spreading rate of the supersonic mixing layer decreases as the Mach number increases.

A lower–upper factored form of the symmetric Gauss–Seidel relaxation method[1] has been widely used in hypersonic flow research since its first applications to nonequilibrium flows.[2–4] The original algorithm employs a fully coupled partially implicit scheme. In theory, robustness of a fully coupled method can be better than that of a loosely coupled method when there is strong interaction between fluid motion and chemical reaction. The fully implicit treatment of the Jacobian might produce less factorization error than the partially implicit scheme. The present paper reports the results from investigation of the effect of modifications to the original algorithm on the stability and convergence for transverse fuel-injection problems in practice.

II. Numerical Methods

Let t be time; $\boldsymbol{Q}$ the vector of conserved variables; $\boldsymbol{E}, \boldsymbol{F}$, and $\boldsymbol{G}$ the convective flux vectors; and $\boldsymbol{E}_v, \boldsymbol{F}_v$, and $\boldsymbol{G}_v$ the flux vectors for the viscous terms. The source term $\boldsymbol{S}$ represents production or destruction of species due to chemical reactions. The three-dimensional Navier–Stokes and species-transport equations in generalized curvilinear coordinates (ξ, η, ς) can be written as

$$\partial_t \boldsymbol{Q} + \partial\xi(\boldsymbol{E} - \boldsymbol{E}_v) + \partial\eta(\boldsymbol{F} - \boldsymbol{F}_v) + \partial\zeta(\boldsymbol{G} - \boldsymbol{G}_v) = \boldsymbol{S} \quad (1)$$

The governing equations are integrated in time for both steady- and unsteady-flow calculations. For a steady–steady solution, the use of a large time step leads to a fast convergence. For a time-accurate solution, it is desirable that the time step be determined by the physics rather than the numerical stability. An unfactored implicit scheme can be obtained from a nonlinear implicit scheme by linearizing the flux vectors about the previous time step and dropping terms of second and higher orders:

$$[I + \alpha\Delta t(D\xi A + D\eta B + D\zeta C - H)]\Delta \boldsymbol{Q} = \text{RHS} \tag{2}$$

where

$$\text{RHS} = -\Delta t[D\xi(\boldsymbol{E} - \boldsymbol{E}v) + D\eta(\boldsymbol{F} - \boldsymbol{F}v) + D\zeta(\boldsymbol{G} - \boldsymbol{G}v) - \boldsymbol{S}] \tag{3}$$

I is the identity matrix, $\Delta\boldsymbol{Q}$ denotes the correction, and A, B, C, and H are the Jacobian matrices of the convective flux vectors and the source term, respectively. Artificial dissipation models augment a piecewise constant cell-centered finite-volume formulation of the right-hand side.[5] One of Jameson's flux-limited dissipation models[3] has been used for calculations in this paper. Let $d_{i+\frac{1}{2}}$ denote the dissipative flux at the cell interface:

$$d_{i+\frac{1}{2}} = -\beta_{i+\frac{1}{2}}\left[\phi\left(\delta\boldsymbol{Q}_{i+\frac{1}{2}} \big/ \delta\boldsymbol{Q}_{i+\frac{3}{2}}\right)\delta\boldsymbol{Q}_{i+\frac{3}{2}} - 2\delta\boldsymbol{Q}_{i+\frac{1}{2}} + \phi\left(\delta\boldsymbol{Q}_{i+\frac{1}{2}} \big/ \delta\boldsymbol{Q}_{i-\frac{1}{2}}\right)\delta\boldsymbol{Q}_{i-\frac{1}{2}}\right] \tag{4}$$

Here ϕ is the flux limiter to limit antidiffusive fluxes and $\delta\boldsymbol{Q}_{i+\frac{1}{2}}$ denotes $\boldsymbol{Q}_{i+1} - \boldsymbol{Q}_i$. The coefficient $\beta_{i+\frac{1}{2}}$ is proportional to a gradient sensor and the spectral radius of flux Jacobian.

Direct inversion of a large block banded matrix becomes impractical in three dimensions because of the rapid increase of computational work and the large storage requirement. The lower–upper symmetric Gauss–Seidel scheme is one of the approximate factorization methods to alleviate the difficulties in three dimensions.

A. Fully Coupled Partially Implicit Scheme

The original algorithm[2] solves the equations in a fully coupled manner. However, the source Jacobian term H has been included in the L factor only. Let us call the algorithm a fully coupled partially implicit scheme. For steady-state solutions, α is set to 1 for all the schemes considered in this paper. The resulting schemes are first-order accurate in time and second-order accurate in space. The diagonals of fluid dynamics equations become scalar if the plus and minus Jacobian matrices of the convective fluxes are constructed using spectral radii.[5] Hence, the resulting scheme requires $(N-1)\times(N-1)$ matrix inversions instead of $(N+4)\times(N+4)$ inversions when N is the number of species:

$$LD^{-1}U\Delta\boldsymbol{Q} = \text{RHS} \tag{5a}$$

where

$$\begin{aligned} L &= I + \alpha\Delta t\left(D_\xi^- A^+ + D_\eta^- B^+ + D_\zeta^- C^+ - A^- - B^- - C^- - H\right) \\ D &= I + \alpha\Delta t(A^+ + B^+ + C^+ - A^- - B^- - C^-) \\ U &= I + \alpha\Delta t\left(D_\xi^+ A^- + D_\eta^+ B^- + D_\zeta^+ C^- + A^+ + B^+ + C^+\right) \end{aligned} \tag{5b}$$

B. Fully Coupled Fully Implicit Scheme

A fully coupled fully implicit scheme can be constructed by including the source Jacobian term in all factors. A linear analysis may suggest that a fully implicit treatment of the source Jacobian introduces less factorization error than a partially implicit scheme although providing more consistent linearization. As in the fully coupled partially implicit scheme, the split Jacobian matrices are constructed approximately using spectral radii to yield diagonal dominance. The scheme requires two $(N-1)\times(N-1)$ inversions and an $(N-1)\times(N-1)$ multiplication:

$$\begin{aligned} L &= I + \alpha\Delta t\left(D_\xi^- A^+ + D_\eta^- B^+ + D_\zeta^- C^+ - A^- - B^- - C^- - H\right) \\ D &= I + \alpha\Delta t(A^+ + B^+ + C^+ - A^- - B^- - C^- - H) \\ U &= I + \alpha\Delta t\left(D_\xi^+ A^- + D_\eta^+ B^- + D_\zeta^+ C^- + A^+ + B^+ + C^+ - H\right) \end{aligned} \tag{6}$$

C. Loosely Coupled Partially Implicit Scheme

Let subscripts f and s indicate fluid and species transport equations respectively. The loosely coupled method solves the Navier–Stokes and species transport equations separately but the solutions are updated simultaneously at each time step:

$$L_f D_f^{-1} U_f \Delta\boldsymbol{Q}_f = \text{RHS}_f \tag{7a}$$

$$\begin{aligned} L_f &= I + \alpha\Delta t\left(D_\xi^- A_f^+ + D_\eta^- B_f^+ + D_\zeta^- C_f^+ - A_f^- - B_f^- - C_f^-\right) \\ D_f &= I + \alpha\Delta t\left(A_f^+ + B_f^+ + C_f^+ - A_f^- - B_f^- - C_f^-\right) \\ U_f &= I + \alpha\Delta t\left(D_\xi^+ A_f^- + D_\eta^+ B_f^- + D_\zeta^+ C_f^- + A_f^+ + B_f^+ + C_f^+\right) \end{aligned} \tag{7b}$$

$$L_s D_s^{-1} U_s \Delta\boldsymbol{Q}_s = \text{RHS}_s \tag{8a}$$

$$\begin{aligned} L_s &= I + \alpha\Delta t\left(D_\xi^- A_s^+ + D_\eta^- B_s^+ + D_\zeta^- C_s^+ - A_s^- - B_s^- - C_s^- - H\right) \\ D_s &= I + \alpha\Delta t\left(A_s^+ + B_s^+ + C_s^+ - A_s^- - B_s^- - C_s^-\right) \\ U_s &= I + \alpha\Delta t\left(D_\xi^+ A_s^- + D_\eta^+ B_s^- + D_\zeta^+ C_s^- + A_s^+ + B_s^+ + C_s^+\right) \end{aligned} \tag{8b}$$

The loosely coupled partially implicit scheme includes the source Jacobian term H only in the L_s factor, as in the fully coupled partially implicit scheme. Solving the equations in a loosely coupled manner ignores such terms in the Jacobian matrix A, for example, as $\partial\boldsymbol{E}_f/\partial\boldsymbol{Q}_s$ and $\partial\boldsymbol{E}_s/\partial\boldsymbol{Q}_f$. Hence, when compared to the fully coupled schemes, the scheme does not need matrix multiplications for off-diagonal terms.

D. Loosely Coupled Fully Implicit Scheme

As in the fully coupled fully implicit scheme, the source Jacobian term H receives a fully implicit treatment in the loosely coupled fully implicit scheme:

$$\begin{aligned} L_s &= I + \alpha\Delta t\left(D_\xi^- A_s^+ + D_\eta^- B_s^+ + D_\zeta^- C_s^+ - A_s^- - B_s^- - C_s^- - H\right) \\ D_s &= I + \alpha\Delta t\left(A_s^+ + B_s^+ + C_s^+ - A_s^- - B_s^- - C_s^- - H\right) \\ U_s &= I + \alpha\Delta t\left(D_\xi^+ A_s^- + D_\eta^+ B_s^- + D_\zeta^+ C_s^- + A_s^+ + B_s^+ + C_s^+ - H\right) \end{aligned} \tag{8c}$$

III. Thermodynamic, Transport-Property, and Finite-Rate-Chemistry Models

In the thermodynamic model, mass-averaged C_p is assumed to be a fourth-order polynomial function of temperature with the coefficients obtained from curve fit data. The gas mixture's C_p is obtained from mass concentration weighting. N is the number of species and Y_i the mass fraction of species i:

$$C_{p_i} = \sum_{k=0}^{4} a_{ik}^c T^k \tag{9a}$$

$$C_{p_m} = \sum_{i=1}^{N} C_{p_i} Y_i \tag{9b}$$

Internal energy of the gas mixture is determined using mixture properties, including enthalpy, which is defined using the reference enthalpy (the heat of formation of species) and the integral of C_p with respect to temperature. Then the temperature is found from the internal energy using Newton iteration because C_p is assumed to be a function of temperature only:

$$e = \sum_{i=1}^{N} Y_i h_i - \frac{p}{\rho} + \frac{1}{2}\sum_{j=1}^{3} u_j^2 \tag{10a}$$

$$h_i = h_{fi} + \int_{T_{\text{ref}}}^{T} Cp_i \, \mathrm{d}T \tag{10b}$$

Pressure is obtained from Dalton's law of partial pressures:

$$p = \rho RT \sum_{i=1}^{N} Y_i / W_i \tag{11}$$

W_i is molecular weight of species i. The equivalent specific heat ratio (sensible enthalpy/internal energy) is used for the Jacobian matrices:

$$\gamma = \frac{\left(\sum_{i=1}^{N} Y_i \int_0^T C_{p_i} \mathrm{d}T\right)}{\left(\sum_{i=1}^{N} Y_i \int_0^T C_{v_i} \mathrm{d}T\right)} \tag{12}$$

In the transport-property model, viscosity and thermal conductivity for individual species are calculated using the fourth-order polynomial expressions

$$\mu_i = \sum_{k=0}^{4} a_{ik}^{\mu} T^k \tag{13}$$

Viscosity and conductivity for the mixture are obtained from Wilkes's mixing rule. X_i and ψ_{ij} denote a mole fraction and an intercollision parameter:

$$\mu = \frac{\sum_{i=1}^{N} \mu_i}{\left[(1/X_i)\sum_{j=1}^{N} X_j \psi_{ij}\right]} \tag{14}$$

Binary mass diffusivity is modeled using the Chapman–Enskog formula for dilute gases in conjunction with Lennard–Jones intermolecular potential energy functions. The intercollision parameter, the effective collision integral factor, and the effective temperature are approximated. The diffusion velocity of each species is calculated using Fick's law and the approximated coefficients for binary diffusion between each species and the mixture.

The source terms represent production or destruction of species due to chemical reactions. The reaction equations for a set of N_R elementary reactions can be written as

$$\sum_{i=1}^{N} \nu'_{ik} C_i \longleftrightarrow \sum_{i=1}^{N} \nu''_{ik} C_i \qquad \text{for} \qquad k = 1, 2, \ldots, N_R \tag{15}$$

Here C_i denotes the mole concentration of species i and ν' and ν'' are stoichiometric coefficients. In the finite-rate-chemistry model, the rate of change of species concentration is defined by the movement of each species summed over all of the contributing reactions (the law of mass action):

$$\dot{\omega}_i = W_i \sum_{k=1}^{N_R} \left[(\nu''_{ik} - \nu'_{ik}) \left(K_k^f \prod_{j=1}^{N} C_j^{\nu'_{jk}} - K_k^b \prod_{j=1}^{N} C_j^{\nu''_{jk}} \right) \right] \tag{16}$$

Forward and backward reaction rate coefficients, K^f and K^b, are calculated from the Arrhenius form. Influence of other bodies on a particular reaction is modeled using a third-body efficiency correction:

$$K_k^f = K_k^f \sum_{i=1}^{N} \tau_{ik} C_i \tag{17}$$

A 9-species, 18-step reaction model[4] for hydrogen and air developed by the NASA Glenn Research Center is adopted. The species considered include H_2, O_2, H_2O, OH, H_2O_2, HO_2, H, O, and N_2.

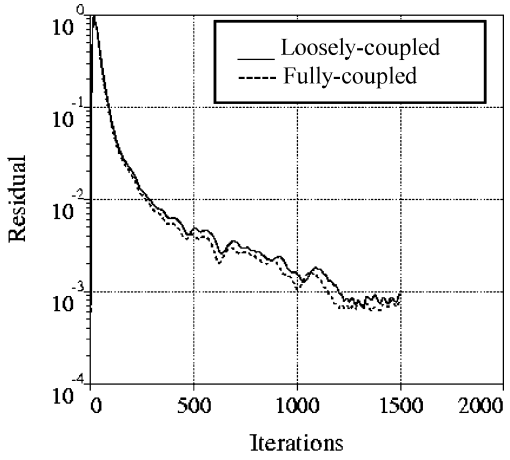

Fig. 1 Convergence histories of the loosely coupled and fully coupled schemes.

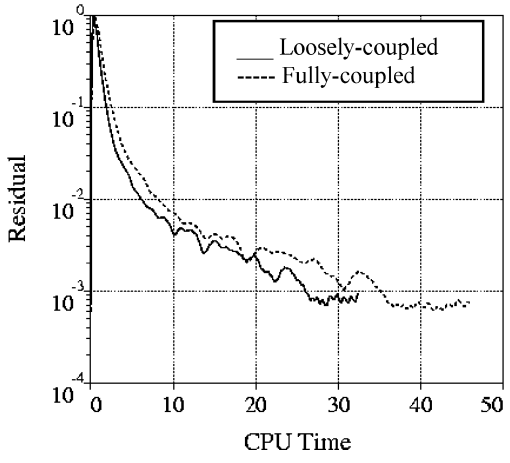

Fig. 2 Computational work of the loosely coupled and fully coupled schemes.

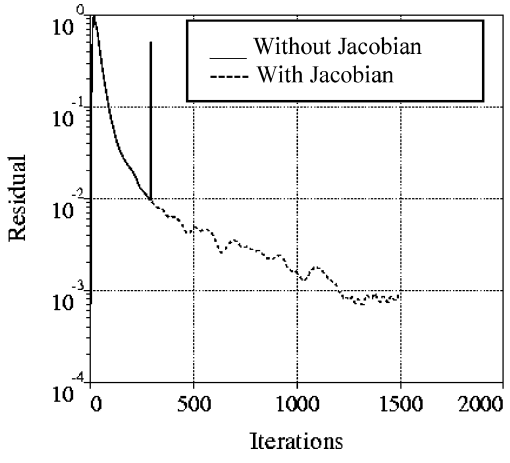

Fig. 3 Convergence histories with and without the implicit treatment of the source term.

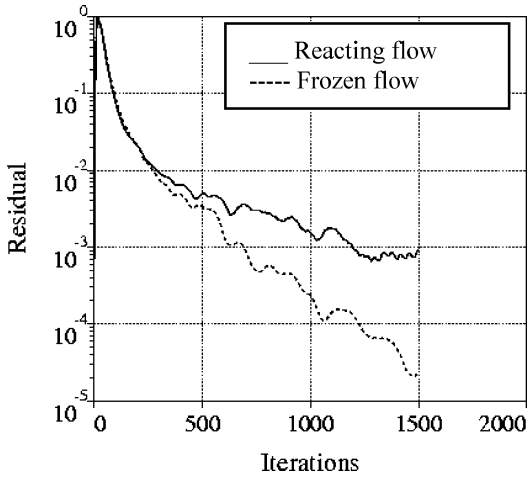

Fig. 4 Convergence histories of reacting and frozen flows.

IV. Results

In the first test case, hydrogen fuel is injected transversely into an incoming supersonic flow of air. The incoming air speed, pressure, and temperature are assumed to be Mach 2, 1 atm, and 1000 K. Gaseous hydrogen is injected at sonic speed through a hole at the bottom whose noncatalytic wall is cooled to 600 K. The length of the combustion chamber is 40 times the diameter of the injector. The Reynolds number based on the length is approximately 10^5. A $257 \times 97 \times 97$ structured grid has been used with symmetric boundary conditions at the top and side walls. Supersonic-flow boundary conditions are imposed at the inlet and outlet planes. Because the validation of a turbulence model is not an objective of the present paper, the Baldwin–Lomax algebraic model[6] has been used for simplicity. In Fig. 1, convergence histories of the loosely coupled partially implicit (solid line) and fully coupled fully implicit (dashed line) schemes are compared. The convergence history of the fully coupled partially implicit scheme is not shown here because it was almost the same as that of the fully coupled fully implicit scheme. Although not shown here, the convergence rates of the fully

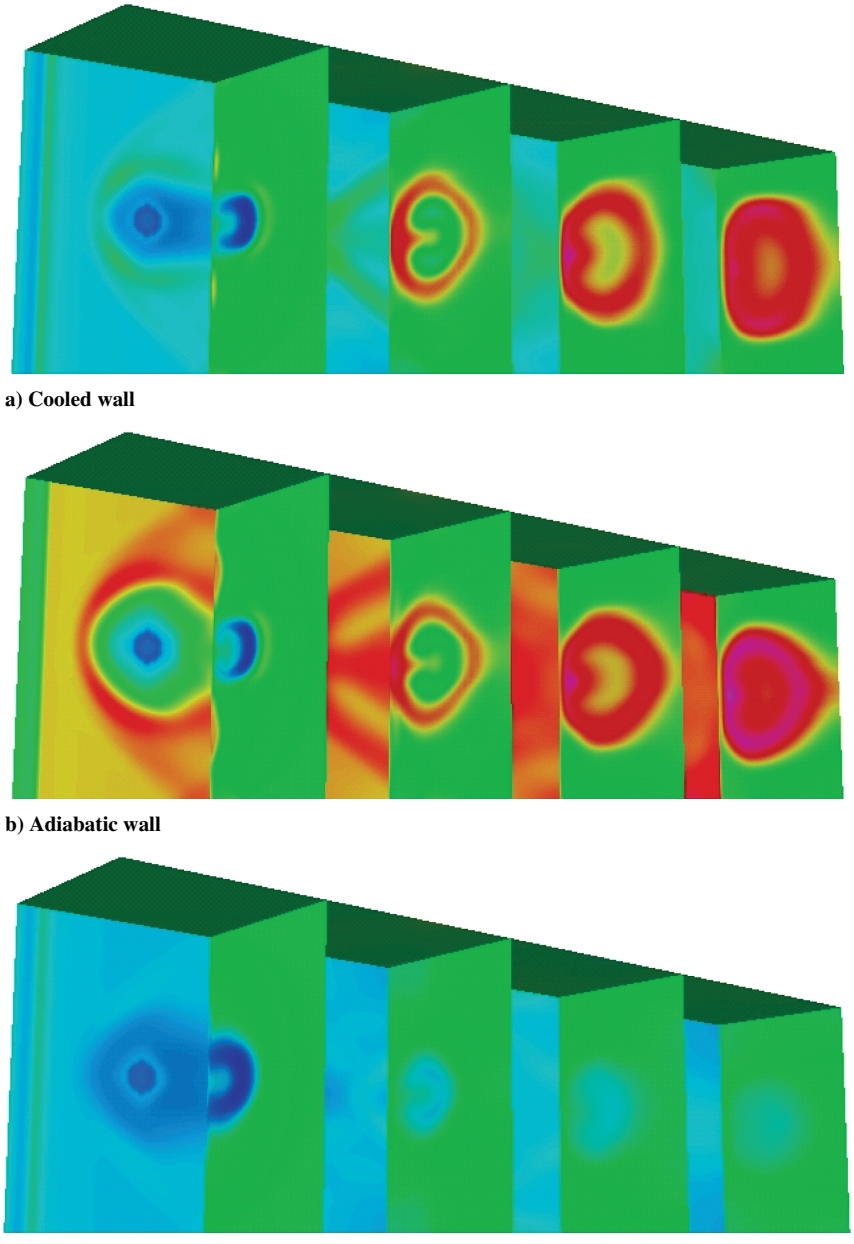

a) Cooled wall

b) Adiabatic wall

c) Frozen flow

Fig. 5 Temperature contours for Mach 2 combustion.

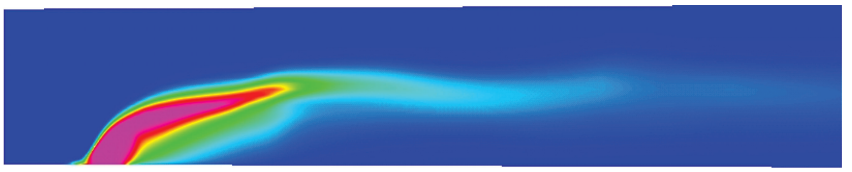

a) H_2

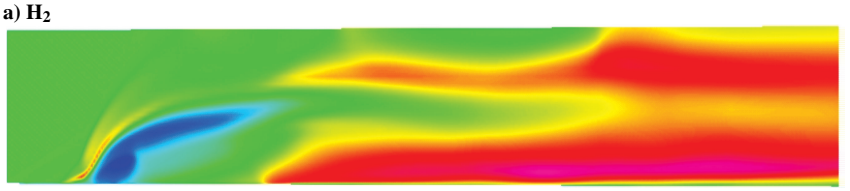

b) Temperature

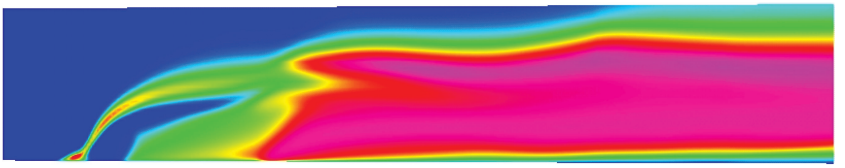

c) H_2O

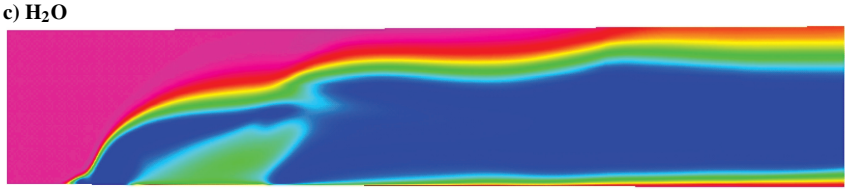

d) O_2

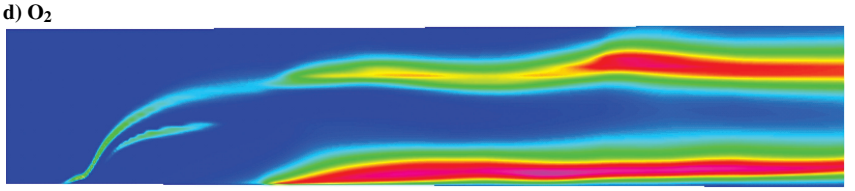

e) OH

Fig. 6 Species mass fraction contours along the centerline for Mach 2 combustion.

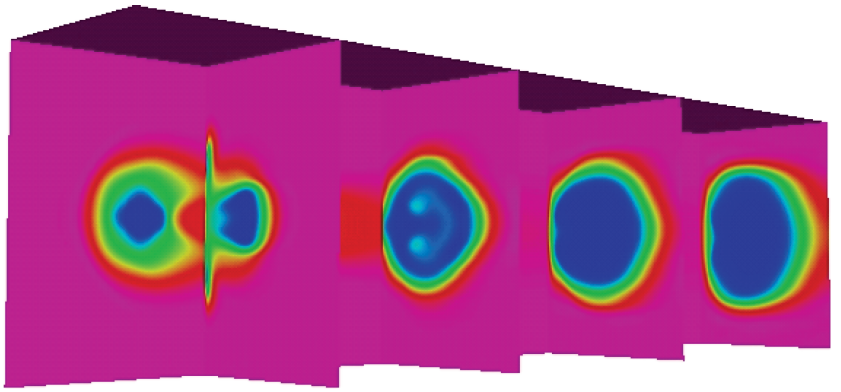

a) Reacting flow

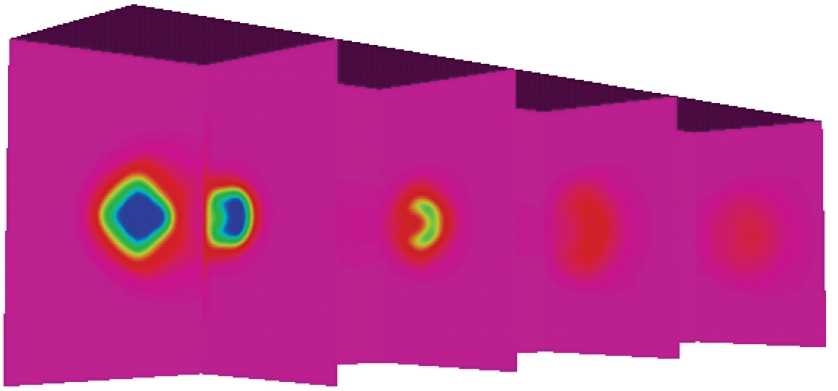

b) Frozen flow

Fig. 7 O_2 mass-fraction contours for Mach 2 combustion.

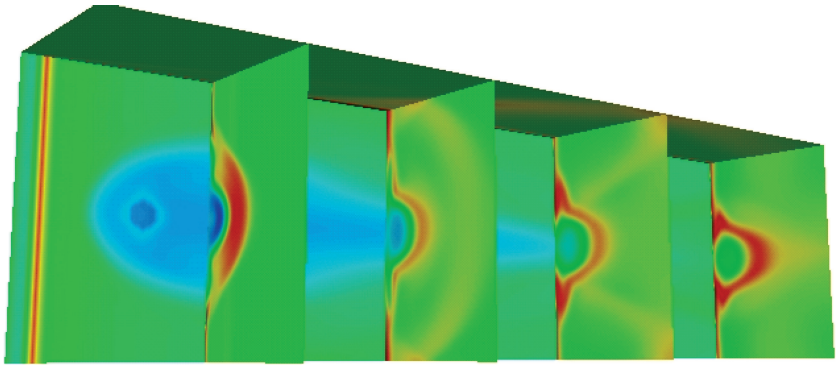

a) Single injection

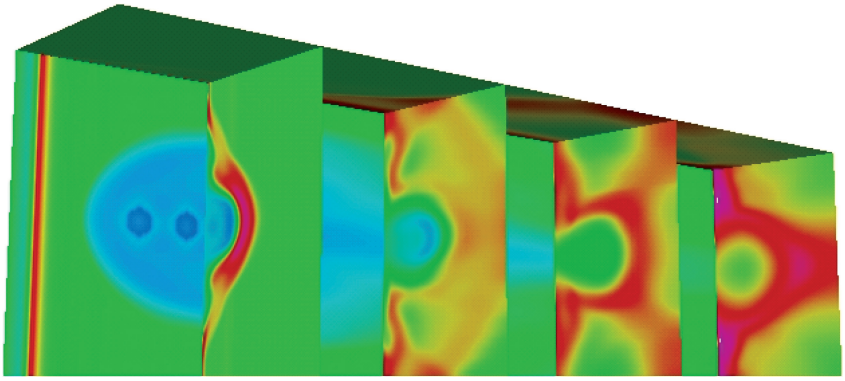

b) Triple-staged injection

Fig. 8 Temperature contours for Mach 4 combustion.

implicit and the partially implicit loosely coupled schemes were almost identical. The difference between fully implicit and partially implicit schemes becomes very small for supersonic flows because the A^- term approaches zero. The numerical method is unconditionally stable and the convergence rates are insensitive to the size of the time step when it is large. A constant time step of $\Delta t = 10$ has been used for all cases. The plot of the L2-norm average of residuals indicates that the convergence rates of both schemes are comparable. However, the computational time per iteration of the fully coupled fully implicit scheme is about 40% greater than that of the loosely coupled partially implicit scheme. In Fig. 2, a comparison of CPU time on a single node of a Cray SV-1 shows that the loosely coupled scheme (solid line) requires less computational work than the fully coupled scheme (dashed line).

The effect of the Jacobian of the source terms on convergence is investigated. In Fig. 3, convergence of the loosely coupled scheme without implicit treatment of the source Jacobian (solid line) shows an almost identical history up to a point and then diverges suddenly. Although the implicit treatment of source terms does not affect convergence rates, it appears necessary for stability. The effect of combustion on the convergence is shown in Fig. 4. The convergence for reacting flow (solid line) is about twice slower than that for nonreacting frozen flow (dashed line).

Figure 5a shows temperature contours for Mach 2 combustion with a cooled wall. The same scale has been used for comparison. The use of the adiabatic wall boundary condition produces increased temperature near the wall, as shown in Fig. 5b. However, the interior flowfield does not appear to be very different from the cooled-wall solution. The frozen flowfield in Fig. 5c shows no temperature rise because there is no chemical reaction. Figures 6a–6e show species mass fraction contours on a plane along the centerline. Consumption of the hydrogen fuel in Fig. 6a and oxygen in Fig. 6d produces H_2O in Fig. 6c and OH in Fig. 6e among others. The bulk of combustion takes place not in the neighborhood of the fuel injector but in the rear part of the chamber. This results in a high-temperature field near the outlet. A comparison of oxygen mass-fraction contours in Fig. 7a and those for the nonreacting flow in Fig. 7b shows the consumption of oxygen clearly.

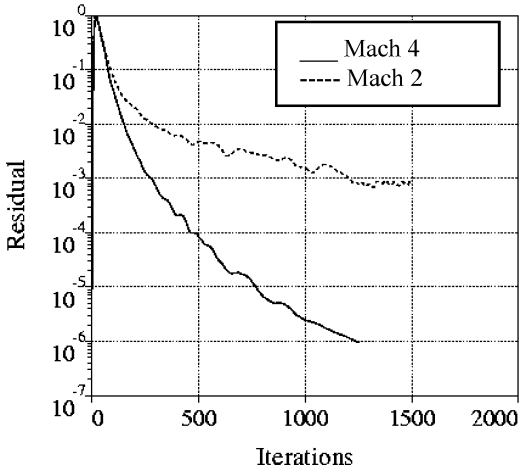

Fig. 9 Convergence histories of Mach 2 and Mach 4 combustion.

When the air speed is increased to Mach 4 at 1300 K, some of the fuel exits without combustion due to insufficient mixing as shown in Fig. 8a. Since there is less combustion than in the case of Mach 2, the convergence appears to be better, as shown in Fig. 9. It has been known that staged multiple injection can enhance combustion efficiency.[7] Figures 8b and 10a show temperature for triple-staged injection where the distance between injector centers is two diameters of the hole. Figures 10b and 10c show increased chemical reaction due to better penetration and enhanced mixing of fuel from the staged injection.

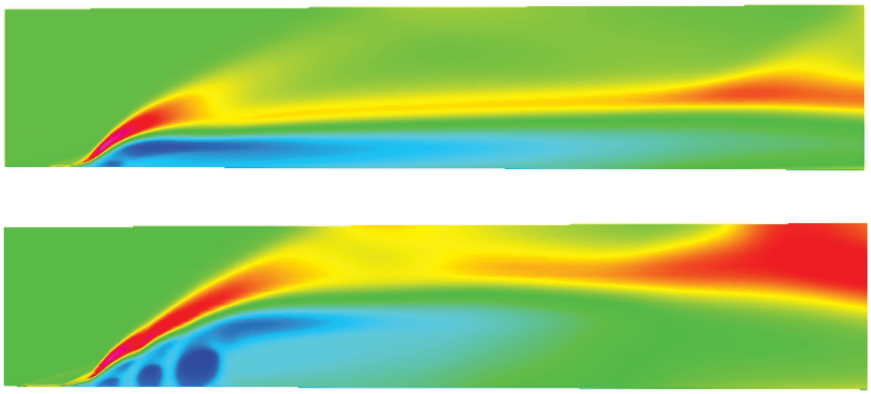

a) Temperature along the centerline

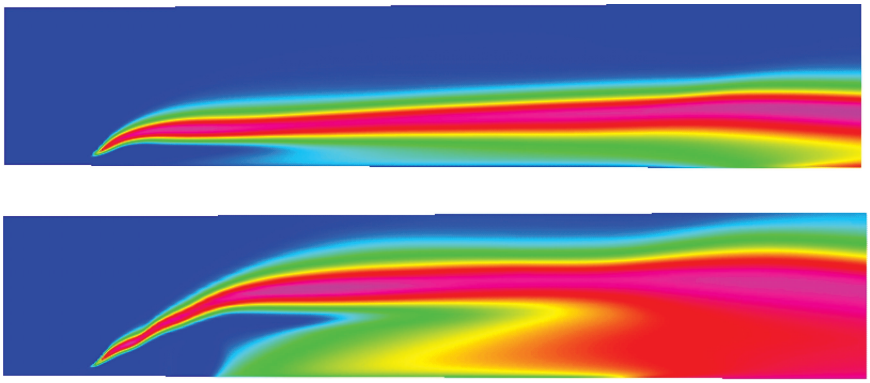

b) H_2O mass fraction along the centerline

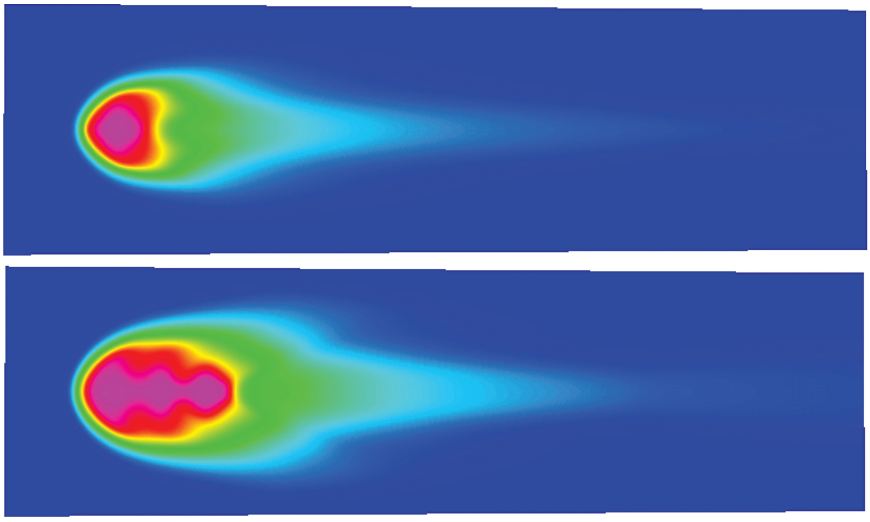

c) H_2 fuel near the bottom wall

Fig. 10 Single and triple-staged injection for Mach 4 combustion

V. Summary

For supersonic combustion, the loosely coupled partially implicit scheme in conjunction with symmetric Gauss–Seidel relaxation provides faster convergence than the fully coupled implicit schemes in terms of computational work. Inclusion of the source Jacobian on the implicit side is only required for stability. It appears that the extent of chemical reaction rather than the speed of flow determines the convergence rates. The robustness of the loosely coupled method has been demonstrated for a staged multiple-injection case.

Acknowledgments

The author thanks T. Pulliam and S. Venkateswaran for helpful discussions.

References

[1]Yoon, S., and Jameson, A., "Lower–Upper Symmetric Gauss–Seidel Method for the Euler and Navier–Stokes Equations," *AIAA Journal*, Vol. 26, No. 9, 1988, pp. 1025, 1026.

[2]Shuen, J. S., and Yoon, S., "Numerical Study of Chemically Reacting Flows Using an LU-SSOR Scheme," *AIAA Journal*, Vol. 27, No. 12, 1989, pp. 1752–1760.

[3]Park, C., and Yoon, S., "Fully-Coupled Implicit Method for Thermochemical Nonequilibrium Air at Suborbital Flight Speeds," *Journal of Spacecraft and Rockets*, Vol. 28, No. 1, 1991, pp. 31–39.

[4]Yu, S. T., Tsai, Y. L. P., and Shuen, J. S., "Three-Dimensional Calculations of Supersonic Reacting Flows Using an LU Scheme," *Journal of Computational Physics*, Vol. 101, No. 2, 1992, pp. 276–286.

[5]Yoon, S., Jameson, A., and Kwak, D., "Effect of Artificial Diffusion Schemes on Multigrid Convergence," AIAA Paper 95-1670, June 1995.

[6]Baldwin, B. S., and Lomax, H., "Thin-Layer Approximation and Algebraic Model for Separated Turbulent Flow," AIAA Paper 78-0257, Jan. 1978.

[7]McDaniel, J. C., and Graves, J., Jr., "Laser-Induced Fluorescence Visualization of Transverse Gaseous Injection in a Nonreacting Supersonic Combustor," *Journal of Propulsion and Power*, Vol. 4, No. 6, 1988, pp. 591–597.

A. Karagozian
Associate Editor

Color reproductions courtesy of the NASA Advanced Supercomputing Division.